Contact Charge Electrophoresis: Experiment and Theory

Aaron M. Drews,[†,‡] Charles A. Cartier,[†] and Kyle J. M. Bishop[*,†]

Department of Chemical Engineering, Pennsylvania State University, University Park, PA, 16802, USA

E-mail: kjmbishop@.engr.psu.edu

Abstract

Contact charge electrophoresis (CCEP) uses steady electric fields to drive the continuous, oscillatory motion of conductive particles and droplets between two or more electrodes. These rapid oscillations can be rectified to direct the motion of objects within microfluidic environments using low-power, dc voltage. Here, we compare high precision experimental measurements of CCEP within a microfluidic system to equally detailed theoretical predictions on the motion of a conductive particle between parallel electrodes. We use a simple, capillary microfluidic platform that combines high-speed imaging with precision electrical measurements to enable the synchronized acquisition of both the particle location and the electric current due to particle motion. The experimental results are compared to those of a theoretical model, which relies on a Stokesian dynamics approach to accurately describe both the electrostatic and hydrodynamic problems governing particle motion. We find remarkable agreement between theory and experiment, suggesting that particle motion can be accurately captured

[*]To whom correspondence should be addressed

[†]Pennsylvania State University

[‡]Current Address: Department of NanoEngineering, UC San Diego, La Jolla, CA, 92093, USA

by a combination of classical electrostatics and low-Reynolds number hydrodynamics. Building on this agreement, we offer new insight into the charge transfer process that occurs when the particle nears contact with an electrode surface. In particular, we find that the particle does not make mechanical contact with the electrode but rather that charge transfer occurs at finite surface separations of $> 0.1\,\mu$m by means of an electric discharge through a thin lubricating film. We discuss the implications of these findings on the charging of the particle and its subsequent dynamics.

Introduction

Contact charge electrophoresis (CCEP) refers to the charging of a conductive particle on contact with an electrode surface and the subsequent motion of that particle in an electric field.[1–3] Unlike other forms of electrostatic or electrokinetic particle manipulation such as dielectrophoresis[4] or induced charge electrophoresis,[5,6] CCEP requires only a static (dc) electric field to produce continuous, oscillatory motion between two electrodes. Simple back-and-forth motion via CCEP has been demonstrated for metallic particles[7–9] and aqueous droplets[10–15] in a variety of insulating fluids including air,[16,17] silicone oil,[11,12] mineral oil,[2,3,8,18] and lighter hydrocarbons such as hexane.[2,19] Importantly, this basic oscillatory motion[20] can be rectified to perform useful functions such as high-speed, directed transport of particles within microfluidic channels[3] as well as efficient, low-power mixing of low Reynolds number streams.[2]

During CCEP, particle dynamics are governed primarily by two processes: contact charging, the acquisition of charge by a conductive particle upon contact with an electrode; and electrophoresis, the movement of the now-charged particle in the applied electric field. Based on classical electrostatics, the charge q acquired by a conductive sphere of radius a on contact with a single plane electrode subject to an applied field E_0 is $q = \frac{2}{3}\pi^3\varepsilon\varepsilon_0 a^2 E_0$, where ε is the dielectric constant of the surrounding medium;[21,22] the presence of a second electrode at finite separation H leads to additional contributions of order $(a/H)^3$.[1] At low particle

Reynolds numbers, the resulting electrophoretic motion may be approximated by equating the electrostatic force $\mathbf{F}_E \approx q\mathbf{E}_0$ to the hydrodynamic drag $\mathbf{F}_H \approx 6\pi\eta a\mathbf{u}$ on the particle as predicted by Stokes law. This simple model provides scaling relationships for the particle charge ($q \sim \varepsilon\varepsilon_0 a^2 E_0$), velocity ($u \sim \varepsilon\varepsilon_0 a E_0^2/\eta$), oscillation frequency ($\omega \sim u/H$), and electric current ($I \sim q\omega$) that have been confirmed through several previous studies.[7–9,16]

To improve upon these approximate scaling relationships, it is necessary to consider the detailed electrostatic[1] and hydrodynamic[23] description of a particle moving between two electrodes. These complementary problems have been solved independently for the case of parallel electrodes using a Stokesian dynamics approach that captures both the far-field, many-body interactions and the near-field (singular) contributions for nearly contacting surfaces.[1,23] These results can be combined to describe the detailed motion of a spherical particle moving via CCEP between parallel electrodes.[1]

Here, we perform high resolution CCEP experiments to assess the validity of the theoretical model and elucidate the details of contact charge transfer. Using synchronized optical and electrical characterization, we collect data on both the particle trajectory $h(t)$ and the instantaneous electric current $I(t)$ accompanying particle motion. These data allow for the validation of both the electrostatic and hydrodynamic models for a spherical particle moving via CCEP at low Reynolds numbers. Extending the electrostatic model to incorporate the effects of electrode curvature, we demonstrate remarkable agreement between the models and the experimental data across the entire inter-electrode region. Interestingly, however, we find that the amount of charge q acquired by the particle on contact is consistently less (*ca.* 66%) than that predicted by theory. We propose a charging mechanism that helps to rationalize these discrepancies and offers new insights on the dynamics of contact charge transfer.

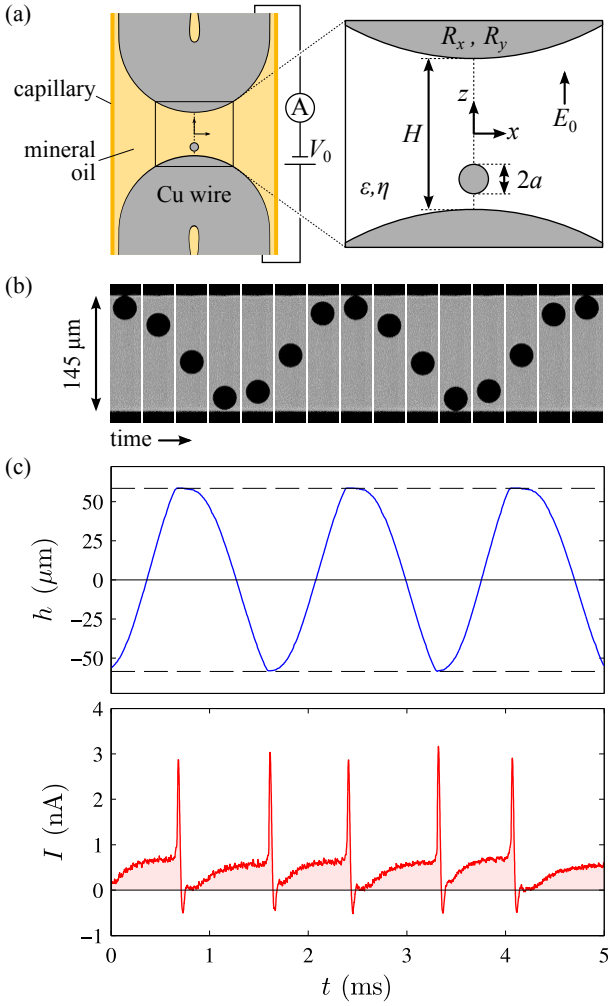

Figure 1: (a) Experimental schematic. A conductive sphere (radius $a = 14\,\mu\text{m}$) is immersed in mineral oil (dielectric constant, $\varepsilon = 2.5$; viscosity, $\eta = 0.027\,\text{Pa}\,\text{s}$) and positioned between two copper wire electrodes separated by a distance $H = 145\,\mu\text{m}$. The curvature of the electrodes is characterized by their two principle radii, $R_x = 510\,\mu\text{m}$ and $R_y = 255\,\mu\text{m}$. Application of a steady electric field $E_0 = V_0/H$ causes the particle to oscillate continuously between the electrodes. (b) Bright-field micrographs taken at regular intervals of $250\,\mu\text{s}$ of a $28\,\mu\text{m}$ particle oscillating at an applied voltage, $V_0 = 765\,\text{V}$. (c) Synchronized particle trajectory $h(t)$ and electrical current $I(t)$ obtained from high speed imaging (*ca.* 10^5 frames per second) and the current preamplifier, respectively, for $V_0 = 765\,\text{V}$.

Experiment

CCEP experiments were conducted within an "off-the-shelf" microfluidic device[24] as illustrated in Figure 1a. Briefly, two copper wires (OD $\approx 0.5\,\mathrm{mm}$) were bent into hairpin geometries and inserted into a square glass capillary through which mineral oil was flowed (Sigma-Aldrich M5904 with measured dielectric constant $\varepsilon = 2.5$ and viscosity $\eta = 0.027\,\mathrm{Pa\,s}$). The entire device was enclosed inside an aluminum Faraday cage to minimize electrical noise and placed under an optical microscope in transmission mode for visualization. During a typical experiment, a suspension of silver-coated hollow glass spheres in mineral oil (Cospheric M-40, $a = 14\,\mu\mathrm{m}$, approximately 0.05 wt% in mineral oil) was flowed into the channel with electrodes energized until a single particle was captured on the electrode surface as observed by optical microscopy. Clean mineral oil, having been filtered *via* $0.45\,\mu\mathrm{m}$ syringe filter, was then used as a purge stream to remove unwanted particles. A single data collection period was initiated by energizing the electrodes to a desired voltage, collecting data, then de-energizing the system for a minimum of one minute before repeating a measurement. Logarithmically-spaced voltages were applied in ascending order from the minimum capable of sustaining reliable oscillation ($V_0 \approx 300\,\mathrm{V}$ or $E_0 \approx 2.1\,\mathrm{V\,\mu m^{-1}}$) to the maximum achievable by the voltage source ($V_0 \approx 1100\,\mathrm{V}$ or $E_0 \approx 7.6\,\mathrm{V\,\mu m^{-1}}$). Each field setting was replicated five times, where each replicate contained approximately 10^2 particle transits between the two electrodes.

Particle location and electrical current data were collected simultaneously by high-speed video (Phantom V310, acquisition at *ca.* 10^5 frames per second) and precision current preamplifier (DL Instruments 1211, rise time $< 250\,\mu\mathrm{s}$) as described previously.[2,3] Importantly, position and electrical data were synchronized to a common start time which corresponds to 1 s after the field was applied. Particle location data were extracted using standard image tracking routines in MATLAB;[25] electrical data were smoothed using MATLAB's cubic smoothing spline function to facilitate further manipulation.

Theory

To describe the motion of a conductive particle moving via CCEP through a dielectric fluid, we require (i) the electrostatic charge q acquired by the particle upon contact with the electrode, (ii) the electrostatic force F_E acting on the charged particle, and (iii) the hydrodynamic drag force F_H that determines its velocity. Here, we review the Stokesian dynamics approach developed previously[1] and extend it to account for the finite curvature of the electrodes.

We consider a conductive sphere of radius a positioned at some point along the shortest path connecting the two curved electrodes (Figure 1a). Owing to the linearity of the Laplace equation, the sphere charge q and dipole moment p are linearly related to the potential on the sphere less the external potential $(\Phi - \Phi^\infty)$ and to the external field (E^∞) at the sphere's center as

$$\begin{bmatrix} q \\ p \end{bmatrix} = \begin{bmatrix} C_{q\Phi} & C_{qE} \\ C_{p\Phi} & C_{pE} \end{bmatrix} \begin{bmatrix} \Phi - \Phi^\infty \\ E^\infty \end{bmatrix}, \tag{1}$$

where $\mathbf{C}$ is the symmetric capacitance tensor ($C_{p\Phi} = C_{qE}$), which can be accurately approximated for the case of two parallel electrodes.[1] Note that the symmetry of the problem ensures that the dipole moment and the electric field are both oriented along the z-direction (*i.e.*, $\mathbf{p} = p\mathbf{e}_z$ and $\mathbf{E}^\infty = E^\infty \mathbf{e}_z$). As described below, knowledge of the external field E^∞ and the capacitance tensor $\mathbf{C}$ enable one to compute all relevant electrostatic quantities such as the charge, force, and current (Figure 2).

To account for effects due to finite electrode curvature, we use the capacitance tensor $\mathbf{C}$ obtained for parallel electrodes but the external potential Φ^∞ and field E^∞ for 'weakly curved' electrodes where the electrode separation is small relative to their curvature ($H \ll R$). In this limit, the potential Φ^∞ and field E^∞ in the absence of the sphere evaluated at

its center ($z = h$) are

$$\Phi^{\infty}(h) = -V_0 \left[\frac{h}{H} + 2\kappa \left(\frac{h^2}{3H^2} - \frac{1}{12} \right) \frac{h}{H} + O(\kappa^2) \right], \quad (2)$$

$$E^{\infty}(h) = E_0 \left[1 + 2\kappa \left(\frac{h^2}{H^2} - \frac{1}{12} \right) + O(\kappa^2) \right], \quad (3)$$

where $E_0 = V_0/H$ is the characteristic field strength, and $\kappa = H(R_x^{-1} + R_y^{-1})/2$ is a dimensionless parameter characterizing the mean curvature of the electrodes (see Supporting Information). This approximation gives the leading order correction to the parallel electrode solution in the limit of weak curvature (Figure 2a).

When the sphere makes electrical contact with either electrode, charge flows to/from the sphere until its potential is equal to that of the electrode (*e.g.*, $\Phi = V_0/2$ for the lower electrode). The equilibrium charge acquired by the sphere can then be computed using equation (1) where the capacitance coefficients are evaluated at contact (*e.g.*, $h \to a - H/2$ for the lower electrode). For the experimental geometry, the equilibrium charge is $q_{eq} = 2.04 q_s$ where $q_s = 4\pi\varepsilon\varepsilon_0 a^2 E_0$ is a characteristic charge scale used throughout the analysis.

The charge on the sphere is balanced by equal and opposite charge, q_l and q_u, distributed over the 'lower' and 'upper' electrodes, respectively, such that $q + q_l + q_u = 0$. The excess charge on the electrodes due to the presence of the sphere can be expressed in terms of the sphere charge q and dipole moment p as

$$q_l = -\left(\frac{1}{2} + \frac{\Phi^{\infty}}{V_0} \right) q + \left(\frac{E^{\infty}}{V_0} \right) p, \quad (4)$$

$$q_u = -\left(\frac{1}{2} - \frac{\Phi^{\infty}}{V_0} \right) q - \left(\frac{E^{\infty}}{V_0} \right) p, \quad (5)$$

as derived in the Supporting Information. The movement of the charged particle across the channel results in the redistribution of this excess charge between the two electrodes via the external circuit. Assuming the sphere charge is constant during its transit from one electrode

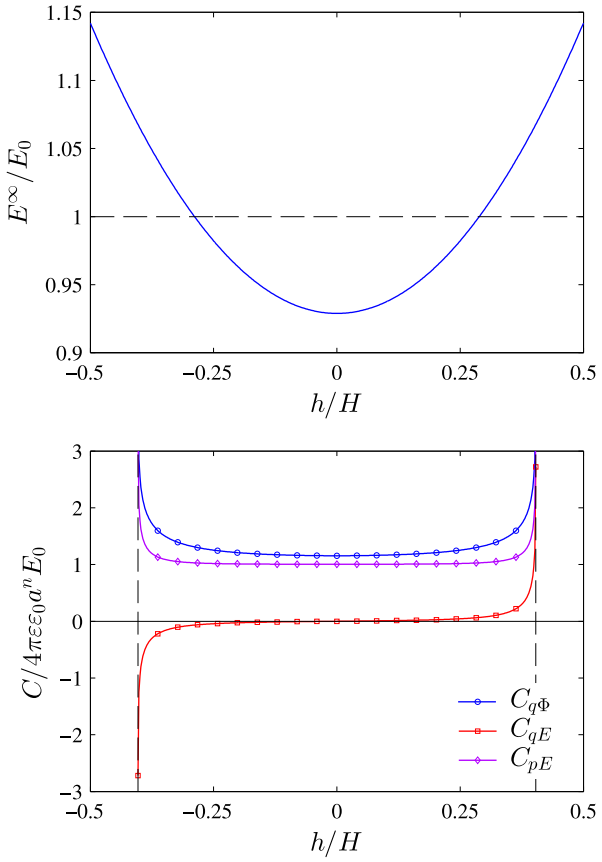

Figure 2: (a). Electric field E^∞ along the axis connecting the two electrodes as approximated by equation (3). Here, the electrode curvature is $\kappa = \frac{1}{2}H(R_x^{-1} + R_y^{-1}) = 0.427$ (as in experiment), and the field is scaled by $E_0 = V_0/H$. (b) Capacitance coefficients as a function of sphere position, h/H, as approximated using the Stokesian dynamics approach.[1] Here, the electrode separation is $H/a = 10.36$ (as in experiment), and the coefficients are scaled by $4\pi\varepsilon\varepsilon_0 a^n E_0$ with $n = 1, 2, 3$.

to the other, the measured current I is related to the sphere velocity $u = dh/dt$ as

$$I = u\frac{dq_l}{dh} = -u\frac{dq_u}{dh}. \tag{6}$$

This relation is used below to estimate the instantaneous charge on the particle from the measured current I and velocity u.

To determine the electric force F_E that drives the motion of the particle, we first compute the electrostatic free energy as

$$U_E = \frac{1}{2}\left(q(\Phi + \Phi^\infty) - pE^\infty\right), \tag{7}$$

assuming that the applied voltage V_0 and the sphere charge q are held constant during its motion across the channel (see Supporting Information). Here, the charge q, the external potential Φ^∞, and field E^∞ are known; the sphere potential Φ and dipole moment p are obtained from equation (1) using the Stokesian dynamics approximation for the capacitance tensor $\mathbf{C}$.[1] The force on the sphere (in the z-direction) can then be computed as

$$F_E = -\left(\frac{dU_E}{dh}\right)_{q,V_0}, \tag{8}$$

where the charge q and the voltage V_0 are held constant.

Neglecting inertial effects, the electric driving force F_E is balanced by a hydrodynamic drag force F_H, which is linearly proportional to the sphere velocity u as

$$F_H = -6\pi\eta a u\lambda(h), \tag{9}$$

where $\lambda(h) > 1$ is a dimensionless factor that describes the increase in hydrodynamic drag due to the presence of the electrodes. This expression is valid in the limit of small Reynolds numbers, $Re = \rho u a/\eta \ll 1$, while the experimental measurements correspond to $Re \approx$

$0.01 - 0.1$. The drag coefficient λ can be accurately approximated using the Stokesian dynamics approach detailed by Swan and Brady[23] for a single sphere between two parallel walls (see below). Importantly, in the absence of external flows (*i.e.*, for a sphere moving in a quiescent fluid), this approximation – which neglects effects due to electrode curvature – is consistent with that used above to evaluate the capacitance tensor $\mathbf{C}$.

Balancing the the electrostatic driving force with the hydrodynamic drag force, we obtain the following dynamical equation for the position of the sphere

$$u = \frac{dh}{dt} = \frac{F_E(q,h)}{6\pi\eta a\lambda(h)}. \tag{10}$$

This equation neglects effects due to particle inertia, which are small relative to the viscous drag as described by the Stokes number, $St = mu/6\pi\eta a^2 \ll 1$, where m is the mass of the particle. In experiments, the silver-coated glass sphere is almost neutrally buoyant, and the Stokes number is similar in magnitude to the Reynolds number, $St \sim Re \ll 1$.

Results and Discussion

Sphere Charge

To determine the charge q on the sphere during each transit, we measured the instantaneous particle velocity u and electric current I when the particle was exactly halfway across the channel (*i.e.*, at $h = 0$). Combined with the theoretical predictions outlined above, these measurements allowed for two independent estimates of the sphere charge. Owing to the symmetry of the electrodes about $h = 0$, the electrostatic force F_E and the electric current I are both linearly proportional to the sphere charge at the center of the channel – that is, $F_E = \alpha q E_0$ and $I = \alpha q u/H$ for $h = 0$ where α is a dimensionless factor computed using the theory outlined above. Note that at other locations in the channel ($h \neq 0$) there are additional contributions to the force and the current due to the field-induced dipole on the

sphere that do not depend on the charge q.

With these preliminaries the charge on the sphere can be estimated from the experimental data as

$$q_h = \frac{6\pi\eta a u \lambda}{\alpha E_0} \text{ and } q_e = \frac{HI}{\alpha u}, \tag{11}$$

where the estimate q_h is based on knowledge of the hydrodynamic drag force, whereas q_e is based on the electric current. Here, the particle velocity u and electric current I are measured experimentally at $h = 0$, the dimensionless parameters $\lambda = 1.38$ and $\alpha = 0.936$ are computed based on theory,[1,23] and the other quantities (η, a, H, V_0) are known. For each applied voltage, we collected five data sets each containing ~200 transits of the particle across the channel; these data were averaged to obtain estimates of the sphere charge q as a function of the applied voltage (Figure 3).

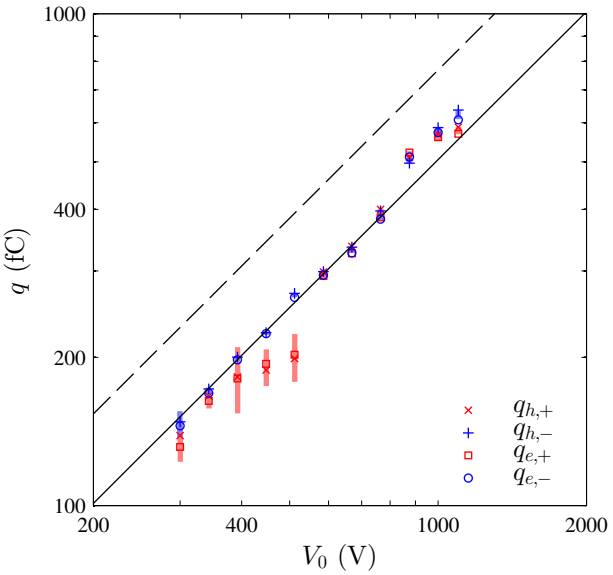

Figure 3: Sphere charge q vs. applied voltage V_0. The charge is estimated using equation 11 (denoted q_h and q_e) for particles traveling in the positive z-direction (denoted +) and the negative z-direction (denoted −). The vertical lines denote 95% confidence intervals on the mean charge. The solid black curve represents the best fit to the data while the dashed curve shows the theoretical prediction.

The data in Figure 3 are divided into four groups based on the method used to estimate the charge (q_h *vs.* q_e in equation (11)) and the direction of travel across the channel (q_+ *vs.*

q_- corresponding to $u > 0$ or $u < 0$, respectively). First, we note that the two independent estimates of the sphere charge agree well with one another (*i.e.*, $q_h \approx q_e$); however, there are often significant variations between the charge acquired on contact with the upper and lower electrodes (*i.e.*, $q_+ \neq q_-$). Importantly, these variations are not due to differences in the sign of the charge q. By changing the polarity of the applied voltage ($\pm V_0$), the sphere acquires positive *or* negative charge of comparable magnitude when it contacts the same electrode (*e.g.*, the upper electrode). Instead, differences between q_+ and q_- are likely due to small imperfections or debri on the electrode surfaces that may influence the charge transfer process (see below).

Aside from these variations, the sphere charge increases linearly with the applied voltage in agreement with model predictions (Figure 3, black curve). Interestingly, however, the measured charge is consistently lower (by $\sim 66\%$) than the equilibrium charge predicted by theory (Figure 3, dashed curve). We[1] and others[9,14,15] have observed similar evidence for incomplete charging in previous studies conducted at low Reynolds numbers ($Re \ll 1$). By contrast, analogous studies performed at high Reynolds numbers (*e.g.*, in air[16] or with mm-sized particles and strong fields[7]) show strong agreement between the measured charge and the predicted equilibrium charge. These observations suggest that hydrodynamic effects may play an important role in the dynamics of charge transfer during sphere-electrode 'contacts' (see below).

Electrostatics

Given the charge on the sphere during each transit, we can use the measured current and position data to rigorously evaluate the validity of the electrostatic model outline above. We first introduce the charge difference, $\Delta q = q_l - q_u$, which measures the difference in the excess charge on the two electrodes due to the presence of the sphere. Using equations (4) and (5)

for the electrode charges, the charge difference is found to depend on the sphere charge q as

$$\Delta q(h) = A(h)q + B(h)q_s, \tag{12}$$

where $A(h)$ and $B(h)$ are dimensionless functions of the sphere position h. Owing to the symmetry of the electrodes about $h = 0$, $A(h)$ is an odd function and $B(h)$ is an even function of the sphere position h. The charge difference can be obtained from experiment by integrating the measured current and making use of equation (6) to obtain

$$\Delta q\left(h(t)\right) = \Delta q(0) + 2\int_{t_0}^{t} I(t')dt', \tag{13}$$

where $h(t_0) = 0$ and the sphere charge q is assumed constant for $t_0 < t' < t$. Here, $\Delta q(0) = B(0)q_s$ cannot be determined directly from experiment and is therefore estimated by theory to be $B(0) = 0.167$ for the present electrode geometry. Using equation 13, we computed the charge difference $\Delta q(h)$ from the measured current at several locations across the channel. This function was then decomposed into odd and even contributions to determine the A and B coefficients presented in Figure 4. The experimental measurements are in excellent agreement with the theoretical predictions. Thus, provided that the sphere is sufficiently far from the electrodes (surface separations greater than a particle radius), its charge remains constant, and the electric force and current are well described by classical electrostatics.

Hydrodynamics

Similarly, we can use equation (10) to estimate the hydrodynamic drag coefficient $\lambda(h)$ as a function of the sphere position h within the channel. Using the measured charge (*i.e.*, the average of estimates q_e and q_h) and the sphere position, the electrostatic force is first computed using equation (8). Equating this force to the hydrodynamic drag force, we then obtain the drag coefficient from the measured particle velocity. The result of this analysis is illustrated in Figure 5 which compares the measured values of $\lambda(h)$ to those obtained

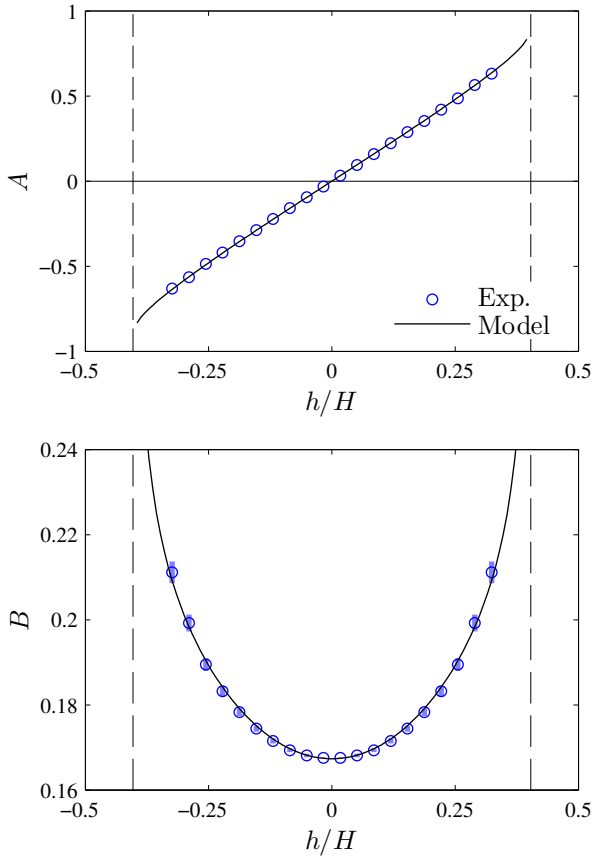

Figure 4: A and B coefficients defined by equation (12). The open markers are experimental measurements; the solid curves are the model predictions. The vertical lines represent 95% confidence intervals on the mean value; confidence intervals for A are smaller than the markers and therefore omitted.

from the hydrodynamic theory for a sphere between parallel walls.[23] There is quantitative agreement between theory and experiment throughout the channel; the small deviations are readily attributed to the effects of electrode curvature neglected by the model.

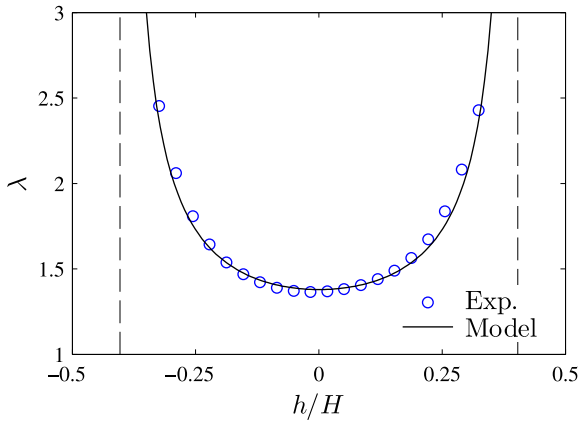

Figure 5: Hydrodynamic drag coefficient λ *vs.* sphere position h. The open markers are experimental measurements; the solid curves are the model predictions.

Contact Charging

Given an accurate description of the physics governing the motion of the sphere across the channel, we now return to the charge transfer process that occurs when the particle 'contacts' the surface of either electrode. Specifically, we consider a charge transfer 'collision' between a negatively charge sphere as it approaches the oppositely biased lower electrode at $z = -H/2$ (Figure 6). During the sphere's approach, the local electric field in the gap separating the the sphere and the electrode begins to rise as $E_{max} \approx (\frac{1}{2}V_0 - \Phi)/(a\xi) \sim E_0/\xi$ where $\xi = (h + \frac{1}{2}H - a)/a$ is the dimensionless surface separation. Eventually, this maximum field exceeds the dielectric strength of the liquid ($E_B \approx 10^7$ V/m for mineral oil), and an electric discharge forms between the sphere and the electrode.[26] Charge then flows rapidly onto the sphere thereby reducing the electric field E_{max} in the sphere-electrode gap. Assuming that some critical field (of order E_B) is necessary to sustain the electric discharge, the trajectory of the sphere through the position-charge phase space is expected to move along a curve of

constant field $E_{max} \sim E_B$ (Figure 6). At some point, however, the electric force F_E on the charged sphere changes sign, and the sphere is pushed away from the electrode surface. The field in the sphere-electrode gap then falls below the critical magnitude necessary to sustain the discharge, and the flow of charge onto the sphere ceases. Importantly, this transition occurs at some finite charge q which is greater than zero, owing to the dielectrophoretic attraction of the sphere to the electrode, but less than the equilibrium charge q_{eq}. For $E_B \approx 30E_0$, the curve of zero force ($F_E = 0$) intersects that of constant field ($E_{max} = E_B$) at a sphere charge of $q \approx 0.5q_{eq}$ – similar to that observed in experiment.

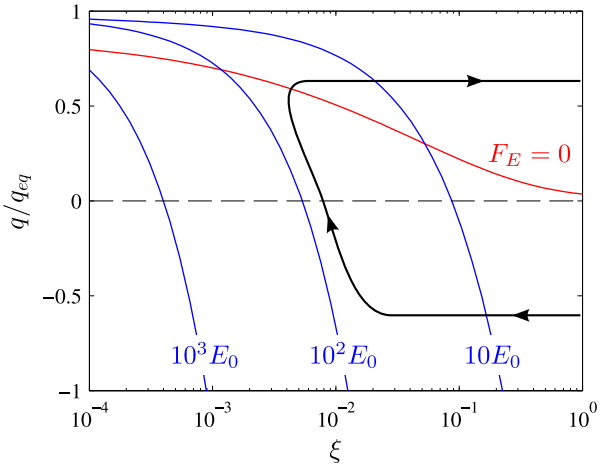

Figure 6: Qualitative particle trajectory (black) through the position-charge phase space. Sphere position is presented as the dimensionless surface separation with the lower electrode, $\xi = (h + \frac{1}{2}H - a)/a$; sphere charge q is scaled by the equilibrium charge q_{eq}. The blue curves show lines of constant electric field E_{max} within the sphere-electrode gap as multiples of the applied field, $E_0 = V_0/H$. The red curve shows the line of zero electric force: $F_E < 0$ below the line (*i.e.*, towards the electrode at $\xi = 0$) and $F_E > 0$ above.

While greatly simplified, this putative mechanism helps to rationalize the experimental observation that the sphere charge never achieves the expected equilibrium value. In the absence of inertial effects, the sphere changes direction immediately upon reversal of the electric force. As a result, the particle does not make mechanical contact with the electrode surface, and charge transfer proceeds *through* a thin lubricating film.

Charge transfer at finite surface separations is further supported by electric current mea-

surements – in particular, by the sharp current 'spikes' that occur when the sphere approaches contact with either electrode. These 'spikes' are typically attributed to the rapid flow of charge between the sphere and the nearby electrode upon dielectric breakdown. However, current 'spikes' may also arise by a purely capacitive mechanism *before* transfer of charge to/from the sphere. When a charged sphere approaches an oppositely biased electrode, the electric current diverges like $I \propto \xi^{-1}$ as the surface separation approaches zero, $\xi \to 0$ (see Supporting Information). This behavior is illustrated in Figure 7a, which shows the electric current predicted by the model for a sphere of constant charge. From the present data, it is difficult to distinguish between these competing hypotheses: the current 'spikes' observed in experiment (Figure 1c) may occur *before* charge transfer as described by the model predictions of Figure 7 or *during* charge transfer *via* dielectric breakdown. Nevertheless, even without detailed knowledge of the charge transfer process, we can apply the capacitive model to determine a lower bound on the surface separation between the sphere and the electrode at 'contact'.

We first determine the average magnitude of the current peaks from the experimental data: $I_{max} = (0.72 \pm 0.05) q_s/t_s$ where $q_s = 4\pi\varepsilon\varepsilon_0 a^2 E_0$ and $t_s = 3\eta/2\varepsilon\varepsilon_0 E_0^2$ are characteristic scales for charge and time, respectively, and the uncertainty represents a 95% confidence interval for all replicates and voltages. Similarly, the average charge on the particle is estimated to be $q = (1.35 \pm 0.02) q_s$. Using this charge estimate, we compute the electric current due to the motion of the sphere via CCEP as shown in Figure 7a. By comparing the results of the model with the peak current measured in experiment, we find that the surface separation at 'contact' must be $\xi_{min} > 0.005$ or roughly 0.1 µm. This order-of-magnitude estimate is consistent with the charge transfer mechanism illustrated in Figure 6. We emphasize that this result is a lower bound since the electric field in the sphere-electrode gap is considerably larger than the breakdown strength at these separations (*i.e.*, $E_{max} \sim 10 E_B$ for $\xi \sim 0.01$). Therefore, charge transfer between the sphere and the electrode likely begins before the current reaches its peak value. Moreover, small surface irregularities

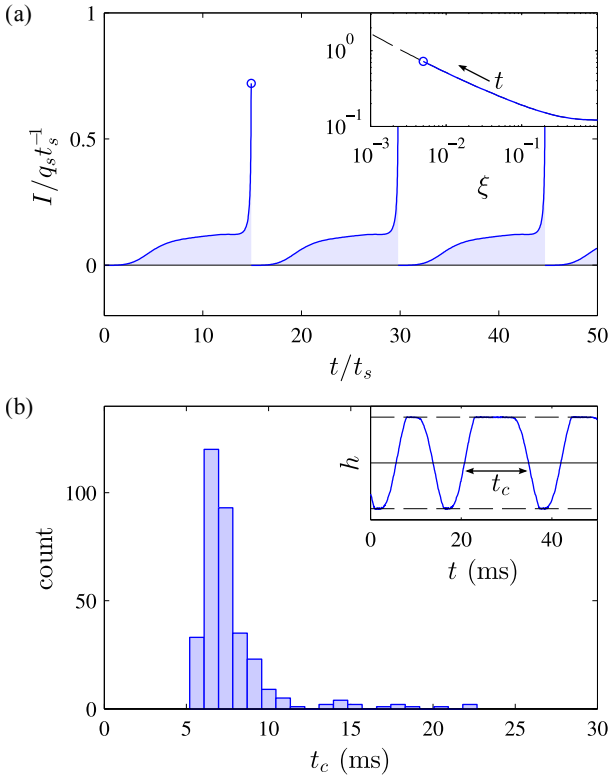

Figure 7: (a) Computed electric current due to the movement of a charged sphere via CCEP. Here, the charge on the sphere is constant and equal to $q = 1.35q_s$ as measured in experiment. The results are presented in dimensionless form using the characteristic scales $q_s = 4\pi\varepsilon\varepsilon_0 a^2 E_0$ and $t_s = 3\eta/2\varepsilon\varepsilon_0 E_0^2$. The inset shows the current as a function of the dimensionless surface separation, $\xi = (h + \frac{1}{2}H - a)/a$. (b) Histogram showing the distribution of 'collision times' t_c (defined in the inset) for the lowest voltage used, $V_0 = 300\,\mathrm{V}$.

on the particle or the electrodes can result in local field enhancements that further promote breakdown, and hence particle trajectory reversal at larger separations $\xi > \xi_{min}$.

Finally, the proposed mechanism for charge transfer has important implications for the dynamics of particles moving via CCEP. First, it helps to explain why the particle sometimes remains near the electrode for a variable period of time before moving off towards the opposite electrode, particularly at weaker fields (Figure 7b). The dynamical trajectory of the particle through the position-charge phase space passes near a fixed point, at which the electric force (and thereby the particle velocity) is zero as is the flow of charge to/from the particle (Figure 6). As a result, there are 'collisions' where the force on the particle is near zero while the viscous resistance to motion is large ($\lambda \sim \xi^{-1} \gg 1$ near contact). Longer times are therefore required for the particle to 'escape' the electrode surface; these times may vary in length due to the stochastic nature of the electric discharges mediating charge transfer.

We also note that because charge transfer occurs at finite surface separations, the role of surface forces between the particle and the electrodes is likely minimal. The particle can oscillate between the two electrodes without ever making mechanical contact with either surface. This result may explain our experimental observation that the minimum voltage required to *initiate* CCEP motions is invariably greater than that required to *sustain* such motions: adhesive surface forces between the particle and the electrode are relevant only during the first charge transfer event. Further experiments are needed to determine the operational limits of CCEP and their origins – in particular, at lower voltages.

Conclusions

We have provided a complete, quantitative description of the electrostatic and hydrodynamic behavior of a particle during contact charge electrophoresis. Building on this accurate description, we provided new and useful insights into the process of contact charge transfer that explains incomplete particle charging and elucidates the nature of particle-electrode

'contacts'. These results can be used to extend our ability to predict particle behavior in new environments. We are currently working to extend the Stokesian dynamics theory to describe the dynamics of multiple interacting particles[27] as well as that of asymmetrically-shaped particles. Such predictive control over CCEP dynamics will help to pave the way towards its application within microfluidic systems and beyond.

Acknowledgement

This work was supported by the National Science Foundation under Grant No. CBET-1351704.

Supporting Information Available

Electrostatic derivations for (1) a conductive sphere between curved electrodes; (2) the electric field between curved electrodes; and (3) the electric current for a particle near contact. This material is available free of charge via the Internet at `http://pubs.acs.org/`.

References

(1) Drews, A. M.; Kowalik, M.; Bishop, K. J. M. Charge and force on a conductive sphere between two parallel electrodes: a Stokesian dynamics approach. *J. Appl. Phys.* **2014**, *116*, 074903.

(2) Cartier, C. A.; Drews, A. M.; Bishop, K. J. M. Microfluidic mixing of nonpolar liquids by contact charge electrophoresis. *Lab Chip* **2014**, *14*, 4230–4236.

(3) Drews, A. M.; Lee, H.-Y.; Bishop, K. J. M. Ratcheted electrophoresis for rapid particle transport. *Lab Chip* **2013**, *13*, 4295–4298.

(4) Zhang, C.; Khoshmanesh, K.; Mitchell, A.; Kalantar-zadeh, K. Dielectrophoresis for

manipulation of micro/nano particles in microfluidic systems. *Anal. Bioanal. Chem.* **2010**, *396*, 401–420.

(5) Squires, T. M.; Bazant, M. Z. Breaking symmetries in induced-charge electro-osmosis and electrophoresis. *J. Fluid Mech.* **2006**, *560*, 65–101.

(6) Gangwal, S.; Cayre, O. J.; Velev, O. D. Dielectrophoretic assembly of metallodielectric Janus particles in ac electric fields. *Langmuir* **2008**, *24*, 13312–13320.

(7) Tobazeon, R. Electrohydrodynamic behaviour of single spherical or cylindrical conducting particles in an insulating liquid subjected to a uniform DC field. *J. Phys. D: Appl. Phys.* **1996**, *29*, 2595–2608.

(8) Khayari, A.; Perez, A. Charge aquired by a spherical ball bouncing on an electrode: Comparison between theory and experiment. *IEEE Trans. Dielectr. Electr. Insul.* **2002**, *9*, 589–595.

(9) Knutson, C. R.; Edmond, K. V.; Tuominen, M. T.; Dinsmore, A. D. Shuttling of charge by a metallic sphere in viscous oil. *J. Appl. Phys.* **2007**, *101*, 13706.

(10) Hase, M.; Watanabe, S. N.; Yoshikawa, K. Rhythmic motion of a droplet under a dc electric field. *Phys. Rev. E* **2006**, *74*, 46301.

(11) Jung, Y.-M.; Oh, H.-C.; Kang, I. S. Electrical charging of a conducting water droplet in a dielectric fluid on the electrode surface. *J. Colloid Interface Sci.* **2008**, *322*, 617–623.

(12) Ristenpart, W. D.; Bird, J. C.; Belmonte, A.; Dollar, F.; Stone, H. A. Non-coalescence of oppositely charged drops. *Nature* **2009**, *461*, 377–380.

(13) Im, D. J.; Noh, J.; Yi, N. W.; Park, J.; Kang, I. S. Influences of electric field on living cells in a charged water-in-oil droplet under electrophoretic actuation. *Biomicrofluidics* **2011**, *5*, 44112.

(14) Im, D. J.; Noh, J.; Moon, D.; Kang, I. S. Electrophoresis of a charged droplet in a dielectric liquid for droplet actuation. *Anal. Chem.* **2011**, *83*, 5168–5174.

(15) Lee, C. P.; Chang, H. C.; Wei, Z. H. Charged droplet transportation under direct current electric fields as a cell carrier. *Appl. Phys. Lett.* **2012**, *101*.

(16) Jones, L.; Makin, B. Measurement of charge transfer in a capacitive discharge. *IEEE Trans. Ind. Appl.* **1980**, *1A-16*, 76–79.

(17) Tuominen, M. T.; Krotkov, R. V.; Breuer, M. L. Stepwise and hysteretic transport behavior of an electromechanical charge shuttle. *Phys. Rev. Lett.* **1999**, *83*, 3025–3028.

(18) Tobazeon, R. Behaviour of spherical and cylindrical particles in an insulating liquid subjected to a DC uniform field. 11th Int. Conf. Cond. Bkdn. Diel. Liq. Baden, CH, 1993; pp 415–420.

(19) Gloos, K.; Schoepe, W.; Simola, J. T.; Tuoriniemi, J. T. Microsphere viscometers for low temperature applications. *Cryogenics* **1992**, *32*, 791–798.

(20) So, J.-H.; Dickey, M. D. Inherently aligned microfluidic electrodes composed of liquid metal. *Lab Chip* **2011**, *11*, 905–911.

(21) Smythe, W. *Static and Dynamic Electricity*; McGraw-Hill: New York, NY, 1950; p 121.

(22) Felici, N. J. Forces and charges of small objects in contact with an electrode subjected to an electric field. *Rev. Gen. L'electricite* **1966**, *75*, 1145–1160.

(23) Swan, J. W.; Brady, J. F. Particle motion between parallel walls: Hydrodynamics and simulation. *Phys. Fluids A* **2010**, *22*, 103301.

(24) Benson, B. R.; Stone, H. A.; Prud'homme, R. K. An "off-the-shelf" capillary microfluidic device that enables tuning of the droplet breakup regime at constant flow rates. *Lab Chip* **2013**, *13*, 4507–4511.

(25) Blair, D.; Dufresne, E. The Matlab Particle Tracking Code Repository. 2010; `http://physics.georgetown.edu/matlab/`.

(26) Tobazeon, R. Prebreakdown phenomena in dielectric liquids. *IEEE Trans. Dielectr. Electr. Insul.* **1994**, *1*, 1132–1147.

(27) Mersch, E.; Vandewalle, N. Antiphase synchronization of electrically shaken conducting beads. *Phys. Rev. E* **2011**, *84*, 061301.

ToC Graphic